Chemical Geology 564 (2021) 120076

Contents lists available at ScienceDirect

Chemical Geology

journal homepage: www.elsevier.com/locate/chemgeo

The in vacuo release of Ar from minerals: 1. Hydrous minerals

Igor M. Villa [a,b,*]

[a] Institut für Geologie, Universität Bern, Baltzerstrasse 3, 3012 Bern, Switzerland
[b] Centro Universitario Datazioni e Archeometria, Università di Milano Bicocca, piazza della Scienza 4, 20126 Milano, Italy

A B S T R A C T

The systematics of Ar release during in vacuo stepwise heating of hydrous minerals is examined. By means of common-denominator three-isotope correlation diagrams, in use for 60 years, it is possible to recognize the presence of polymineralic mixtures in a step-heated mineral separate and characterize their components. These correlation diagrams, when applied to literature studies proposing Fick's Law diffusion during in vacuo stepwise heating, show that in actual fact these studies were based on partly retrogressed micas that were intergrown with their alteration products, probably at a scale < 20 μm so as to escape recognition during handpicking. The degassing of hydrous minerals in vacuo does not follow Fick's Law in an inert, homogeneous matrix, and instead proceeds from the structural collapse during dehydration. An alternative presentation discussed here quantifies the differential release of the Ar isotopes. Their release follows the structural collapse of their host phases and gives rise to remarkably well resolved patterns even in polymineralic samples.

Not all theories deserve equal time.

(Naomi Oreskes, *The Rejection of Contiental Drift*)

1. Introduction

It is a common observation that minerals used as K—Ar chronometers degas Ar at different temperatures in the laboratory. The first attempts to understand rare gas release from minerals during in vacuo stepwise heating (e.g. Reynolds, 1963) were a phenomenological description of the "typical" temperatures of degassing. Initially the rare gas most intensively investigated was Xe in meteorites; differential Xe release was understood to be an indicative property of the carrier phases hosting isotopically distinct Xe components, which came to be recognized as very different nucleogenetic signatures. Over the following decades, the carrier phases of exotic Xe (microdiamonds, silicon carbide, etc) have been identified petrographically and linked to specific presolar nucleosynthetic events. The match between the petrography of very elusive trace minerals with the indication of distinct carrier phases of isotopically distinguishable rare gas components validates the Reynolds (1963) approach.

It has long been documented that hydrous minerals such as micas (Zimmermann, 1970; Sletten and Onstott, 1998) and amphiboles (Gaber et al., 1988) dehydrate in vacuo. The connection between the dehydration and the Ar release, and the interpretive constraints it provides when applied to typical terrestrial minerals, is the focus of the present paper.

2. Bruderheim: the archetype of a momentous misunderstanding

The archetype on which all interpretations of ^{39}Ar—^{40}Ar age spectra were based for about 30 years, and which is still revered by many users to the present day, is the Bruderheim meteorite. The full data were never made public, but were graphically displayed by Merrihue and Turner (1966).

The Berkeley rare gas laboratory (Reynolds, 1963) had analyzed dozens of meteorites in their quest for an evolutionary history of the Early Solar System, making use of a presentation scheme based on common-denominator three-isotope correlation plots (hereafter CDTIC). In such diagrams some points representing individual heating steps would align along linear trends; the end-points of the respective segments were either well-documented components, such as Xe deriving from fission of ^{235}U, ^{238}U, ^{244}Pu (which had all been extensively documented in the wake of the Manhattan project), or inferred components, such as spallation Xe produced by cosmic rays or the "Average Carbonaceous Chondrite Xe" calculated after deconvolution from other Xe components (Reynolds, 1963). A key observation was that Xe deriving from different cosmochemical processes (obviously located in chemically different mineral phases) was released at different furnace

* Institut für Geologie, Universität Bern, Baltzerstrasse 3, 3012 Bern, Switzerland, Centro Universitario Datazioni e Archeometria, Università di Milano Bicocca, piazza della Scienza 4, 20126 Milano, Italy.
E-mail address: igor@geo.unibe.ch.

https://doi.org/10.1016/j.chemgeo.2021.120076
Received 12 October 2020; Received in revised form 11 January 2021; Accepted 15 January 2021
Available online 19 January 2021

temperatures in the laboratory (Reynolds, 1963, his Figs. 8–10). Especially foreboding was the reference (Reynolds, 1963, p. 2949) to a paper to be published by Merrihue on the rare gas systematics in an irradiated Bruderheim sample. The Ar part of these data was presented, after Merrihue's death in 1965, by Merrihue and Turner (1966) by resorting to the well-tested CDTIC plots; one such correlation plot (Merrihue and Turner, 1966, their Fig. 5) was the analog of the slightly earlier proposed Rb—Sr isochron diagram (Allsopp, 1961; Nicolaysen, 1961) and yielded the apparent K—Ar age of each heating step.

Subsequent papers by Turner et al. (1966) and Turner (1968) presented a different interpretation of the Bruderheim data. The CDTIC were abandoned in favor of the "age spectrum" presentation. Turner (1968) modelled the Bruderheim chondrite as consisting of a lognormal population of monomineralic spheres, whose degassing in space and in the laboratory yielded a monotonically rising age spectrum. In the age spectrum presentation the information provided by the CDTICs available for the five Ar isotopes (which represent the distribution of datapoints in 4-dimensional space) is projected onto the 2-dimensional plane defined by three Ar isotopes (^{40}Ar, ^{39}Ar, ^{36}Ar), with attending massive loss of information. It is therefore not surprising that the interpretation of the Bruderheim meteorite as a monomineralic system was antithetic to its mineralogical diversity. The latter had been presented in two papers, which dealt explicitly with the mineral assemblage of Bruderheim and quantified the modal proportions of plagioclase, pyroxene and other Ca- and K-free minerals (Baadsgaard et al., 1961; Duke et al., 1961). When taking into account the degassing systematics of noble gases hosted by different carrier minerals (i.e., multicomponent) established by Reynolds (1963), the interpretation that forces itself from the Bruderheim data is that chondrites do not consist of monomineralic spheres, distributed lognormally or otherwise, but instead consist of different minerals, whose degassing temperatures are different, sometimes extremely well separated (as initially described by Merrihue and Turner, 1966, their Fig. 3).

Bruderheim in fact provides a prime example of the Ar—Ar discordance systematics as reviewed by Villa and Hanchar (2017): its discordance is explained (Merrihue and Turner, 1966, their Fig. 3) by the sequential degassing of a 500 Ma old K-rich, Ca-poor phase (maskelynite? matrix? feldspar?) and a > 3000 Ma old Ca-rich, K-poor phase (anorthite? pyroxene?). Unfortunately for the scientific community, the 1968 interpretation of the Bruderheim data spawned the misinterpretation of discordant age spectra as representing diffusion, a misconception still deeply rooted in many publications on geochronology - despite the definitive evidence by Turner et al. (1971) that this is untrue. These latter authors demonstrated that the "staircase shape" of the age spectrum of lunar sample 14053 was not an intrinsic property of the rock, as it was nearly eliminated by mineral purification by handpicking. The staircase of 14053 therefore could not be viewed as recording "diffusive" Ar loss from a monomineralic system (see the discussion by Villa and Hanchar, 2017, their Fig. 5) but instead as the degassing of two quite different mineral phases: a young one (the so-called mesostasis, or fine-grained matrix abundant in lunar rocks, usually attributed to continuous gardening by micrometeorite impacts) and one or more older crystalline phases, such as plagioclase and pyroxene.

3. Polymineralic mixtures: how to unravel diachronous mineral growth episodes

The polymineralic nature of the Bruderheim archetype could, at first sight, be considered irrelevant for an ideally pure separate of an ideally homogeneous terrestrial mineral. After all, mineralogy textbooks describe a world of stoichiometric phases. However, especially after the introduction of electron probe microanalysis (EPMA), it is ubiquitously observed that internationally circulated reference materials used as irradiation monitors, and a fortiori the ordinary rocks analyzed in most real-world geochronology studies, respect neither ideal stoichiometry, nor ideal homogeneity, nor ideal absence of other over−/intergrown phases (e.g. Hall, 2014, his Table 4); this holds true even for museum specimens (Naumenko-Dèzes et al., 2018). The questions then must be: (i) what other phases can be present in a K-bearing mineral used for dating; (ii) what age information can be gained from a convolved, polymineralic and polygenetic system.

The minerals most commonly used in K—Ar geochronology are amphiboles, feldspars, and micas. The behaviour of amphiboles during in vacuo stepwise heating has been clarified over twenty years ago (Villa et al., 1996, 2000). It is accepted without doubt that amphiboles react and decompose in vacuo (Wartho et al., 1991; Lee et al., 1991; Lee, 1993; Wartho, 1995) in coincidence with major bursts of Ar degassing. As most amphiboles are K-poorer than feldspars and micas, minor inclusions of K-feldspar and/or mica tend to have large effects on the chemical signature revealed by the $^{37}Ar_{Ca}/^{39}Ar_K$ and $^{38}Ar_{Cl}/^{39}Ar_K$ ratios (Villa et al., 1996), which reflect the Ca/K and Cl/K ratios. These chemical ratios can on one hand be validated by EPMA, and on the other hand provide a chemical characterization of the phase(s) degassed in a particular heating step. The remarkable compositional variability of amphiboles can be used as a thermobarometer (Raase, 1974), enabling the reconstruction of a *P-T-t* segment (e.g., Villa et al., 2000). If, moreover, the phases intergrown with amphibole are diachronous retrogression products, the age spectrum becomes discordant (Villa and Hanchar, 2017), whereby a CDTIC plot can routinely reveal the composition and the age of the contaminant phase(s).

Feldspars have a high ionic porosity (Dahl, 1997, his Table 1), which makes them very reactive with aqueous fluids. Retrograde reactions ("deuteric coarsening" of Parsons et al., 1999) are ubiquitous, resulting in at least partial alteration to kaolinite, as well known to the ceramics industry (e.g. Pruett and Pickering Jr, 2006). A reexamination of the petrology of the original archetype used for Ar diffusion modelling, the Chain of Ponds microcline MH-10 (Lovera et al., 1993), was performed by Chafe et al. (2014) using cathodoluminescence and transmission electron microscopy as a prerequisite for ^{39}Ar—^{40}Ar analysis. It demonstrated that the MH-10 "K-feldspar" actually consists of clays, μm-sized celsian veins, hydrothermal adularia, (relict?) plagioclase, and magmatic K-feldspar, whereby each of the first three minerals represents a diachronous reaction on the retrograde path. A side-effect of the petrographic analysis of MH-10 was the recognition that Lovera et al. (1993) had actually estimated the diffusivity of K-feldspar from the degassing rate of clayey alteration minerals.

Muscovite and biotite have very wide stability fields, which means that they can grow above or below their "closure temperature" for Ar diffusion (see the definitions and discussion in Villa, 2016). This makes the interpretation of mica K—Ar ages decisively dependent on microstructural, microchemical and petrological groundwork, without which the conclusions inferred from arbitrary modelling are unfounded. Texturally controlled electron microprobe element maps such as discussed by Villa and Hanchar (2017, their Fig. 9) are the only way to assess how many mica generations were formed in how many deformation and/or static reaction events. Different biotite generations can have variable Cl/K signatures, but should have Ca/K = 0 (unless they are retrogressed to chlorite or pyrophyllite, which characteristically gives substoichiometric Na + K concentrations and high apparent Ca/K > 0). Exotic micas (e.g. clintonite, fuchsite) have only rarely been dated. In the more frequent white mica varieties (phengite, muscovite, paragonite) variable Ca and Cl substitutions are documented (Allaz et al., 2011; Villa et al., 2014), which makes the use of CTDIC a powerful tool to match the microstructural observations with an age estimate.

4. The elephant in the room: diffusion?

Fick's Law diffusion always occurs, as all atoms always move at $T > 0$ K. The question is therefore: how fast does it occur, and in which cases can one quantify its evidence in geological materials? Do Arrhenius diagrams obtained in laboratory experiments provide any indication of diffusion rates?

Firstly, it must be emphasized that Arrhenius diagrams display the temperature dependence of the rate constant, $k(T)$, of any temperature-dependent process. If, and only if, the only process occurring in a given system is Fick's Law diffusion, then the rate constant k coincides with the frequency factor D/a^2. If a can be measured, the diffusion constant D can be determined. In the general case, however, k is not per se an accurate estimate of the diffusion constant, as more than one process (e.g. advection and diffusion) can be operating at the same time, or the studied temperature-dependent process (e.g. a chemical reaction) can be totally unrelated to diffusive transport. The implication arrow is one-sided: if diffusion occurs alone, then an Arrhenius diagram returns the diffusion constant. If a rate constant is measured, then it cannot be concluded that $k = D/a^2$.

In natural geochronometers under metamorphic conditions Fick's Law diffusion can be detectable (or even predominant) in exceptional cases (Allaz et al., 2011; Villa et al., 2014, p. 816). However, owing to the relative rate of diffusion versus that of coupled aqueous dissolution-reprecipitation (Villa, 2016), in the overwhelming majority of geological situations the latter vastly predominates over the former (Airaghi et al., 2018; Bosse and Villa, 2019; Akker et al., 2021).

Even if during the geological history of natural samples diffusion is overrun by faster retrograde reactions, in vacuo degassing of minerals in the laboratory occurs in the absence of water, and dissolution-reprecipitation is not a viable process. Thus, it could be conceivable that Ar release during stepwise heating did follow Fick's Law. In the present paper, the evidence pertaining to hydrous phases, especially micas, will be reviewed.

Prima facie evidence for the Ar release from hydrous minerals is that their degassing rate deviates from linearity in Arrhenius plots (Gaber et al., 1988). The mathematical construction to salvage the assumption of Fickian degassing is to add a second assumption, namely that hydrous minerals in crystallographic continuity are not really continuous but consist of discrete "domains". This generalizes the assumption that Lovera et al. (1993) proposed for K-feldspars to also apply to hydrous minerals (Harrison et al., 2009; Kula and Spell, 2012). Even if it is now established that the Lovera et al. (1993) model is based on overlooking petrological reality (Chafe et al., 2014), one possibility still could be open: are amphiboles and micas different from K-feldspar, in such a way that their in vacuo degassing is compatible with a Fickian description of Ar release?

The mechanisms of Ar release from amphiboles are not controversial, as they clearly proceed from breakdown reactions (Villa et al., 1996, and references therein; see also below). As for micas, the time-scale and sequence of the crystallographic processes that accompany dehydration at the atomic scale have not yet been completely studied. It is likely, but as yet unproven, that when the dehydration reaction ($2\ OH^- \leftrightarrow H_2O + O^{2-}$) occurs in the octahedral layer of micas, the expulsion of the water molecules requires the transient formation of vacancies, which may be large enough to allow the rapid removal of most Ar atoms. If this causes a displacive transformation (sensu Laves, 1956), then crystallographic analyses at room temperature cannot detect the crystallographic scar of the reaction. This suggestion might reconcile two apparently contrasting observations: the interlayer distance after dehydration appears unmodified, yet the most prominent burst of Ar degassing (see below) occurs precisely in temperature interval of dehydration. The dehydration and ensuing structural reshuffling of the TOT framework results in a well known effect: step-heated mica samples independently known to have a zoned intra-grain Ar distribution yield plateaus (Foland, 1983; Hodges et al., 1994) or at most very subdued quasi-plateaus (Phillips and Onstott, 1988).

Harrison et al. (2009) instead incur in a fundamental misunderstanding: they equate the shape of discordant age spectra with concentric $^{40}Ar^*$ zoning resulting from diffusive loss. They model the ^{39}Ar release so as to make the data compatible with Fickian diffusion out of a homogeneous mineral consisting of a collection of discrete "domains". Their argumentation is a prime example of the Brandolini principle (Bergstrom and West, 2020, p.11). However, their theoretical model is not only inconsistent with established mineralogical knowledge, it is also internally inconsistent when considered in detail. First of all, the TEM evidence by Hess et al. (1987) on hydrothermally heated muscovite disambiguates the staircase-shaped age spectra: they reflect the formation of secondary reaction products. The presence of secondary reaction products was downplayed by Harrison et al. (2009, their Fig. 4), who presented but ignored the evidence that all of the treated samples had compositions midway between the starting composition of the white mica ([Si] = 3.12–3.14 atoms per formula unit, apfu) and that of the most evident recrystallization products ([Si] = 3.02–3.05 apfu). Coupled dissolution-reprecipitation was not an "occasional, minor disturbance" but the dominant process accounting for the compositional difference between starting material and treated samples, whereby practically none of the treated samples was exempt from open-system chemical reactions (Fig. 1). Since no measurement of the Cl/K ratio was obtained, the most reliable discrimination of secondary muscovite from the more phengitic starting material was not available. The observational proof is that the runs in both the identically designed Hess et al. (1987) and Harrison et al. (2009) experiments were not controlled by temperature-dependent diffusion but by some other, temperature-independent process which predominated over Fickian diffusion. Such a process, as documented by the Si—Al exchange and by the ubiquitous formation of "very fine, euhedral, neoformed grains" (Célérier, 2007, p. 163), was coupled dissolution-reprecipitation. By mass balance, a run product grain having [Si] = 3.08 apfu is a mixture of 33% starting material (having [Si] = 3.14 apfu) and and 67% reaction precipitate (having [Si] = 3.05 apfu). The implication is that even the most extreme Ar loss recorded by the 730 °C runs, $f = 0.651$ (Célérier, 2007, Table 6.2), could very well be entirely explained by the observed dissolution-reprecipitation, leaving true Fick's Law diffusion loss near, or even equal to, zero.

It is not surprising that muscovite dissolves and then reprecipitates in a hydrothermal experiment in the laboratory, as biotite certainly does, both at the 10-μm scale and at the sub-μm scale (Villa and Puxeddu, 1994, their Fig. 3). The relative importance of this additional, faster reaction on the intended determination of true Fick's Law diffusivity is enhanced at low fractional losses, i.e. at lower experimental temperatures, such that the activation energy, given by the slope of the Arrhenius regression, is both less precise and less accurate (Villa, 2010, p. 5–6). The effect of only modelling Ar loss by Fick's Law diffusion, neglecting the observation of faster reactions, is that the long extrapolation to geological temperature conditions is modelled with an incorrect slope.

All the data used in the following discussion were taken from the original PhD thesis by Célérier (2007). It is essential to note that the Supplementary Data of Harrison et al. (2009) differ in several respects from those in the PhD thesis. The journal paper presents different isotope concentrations and ratios than the PhD thesis, the only agreement being the step ages and the cumulative ^{39}Ar release. Further, Célérier (2007) reports the primary experimentally measured quantity, fractional loss, f, whereas Harrison et al. (2009) report instead of f a different quantity, the Fourier number F modelled for the "large domain". This makes it impossible to check whether the dependence of f on the run time t (Harrison et al., 2009, their Fig. 11) actually obeys the equations governing Fick's Law. In fact, none of the six numeric values of f plotted by Harrison et al. (2009, their Fig. 11) agree with the three f values measured by Célérier (2007, Table 6.2 and Fig. 6.10) on the only set of mutually comparable experiments, namely the three 10 kb runs performed at 730 °C on 24 μm grain radius with alumina buffer and not rejected by the experimenter. When the apparent diffusion constant D is plotted as a function of fractional loss f (both as given by Célérier, 2007) one can observe (Fig. 1c) that there is a negative correlation. Since by definition D is constant in aliquots of the same sample, an explanation is needed. The first point to keep in mind is that D is not directly measured. The measured quantity is the fractional Ar loss, f. This quantity

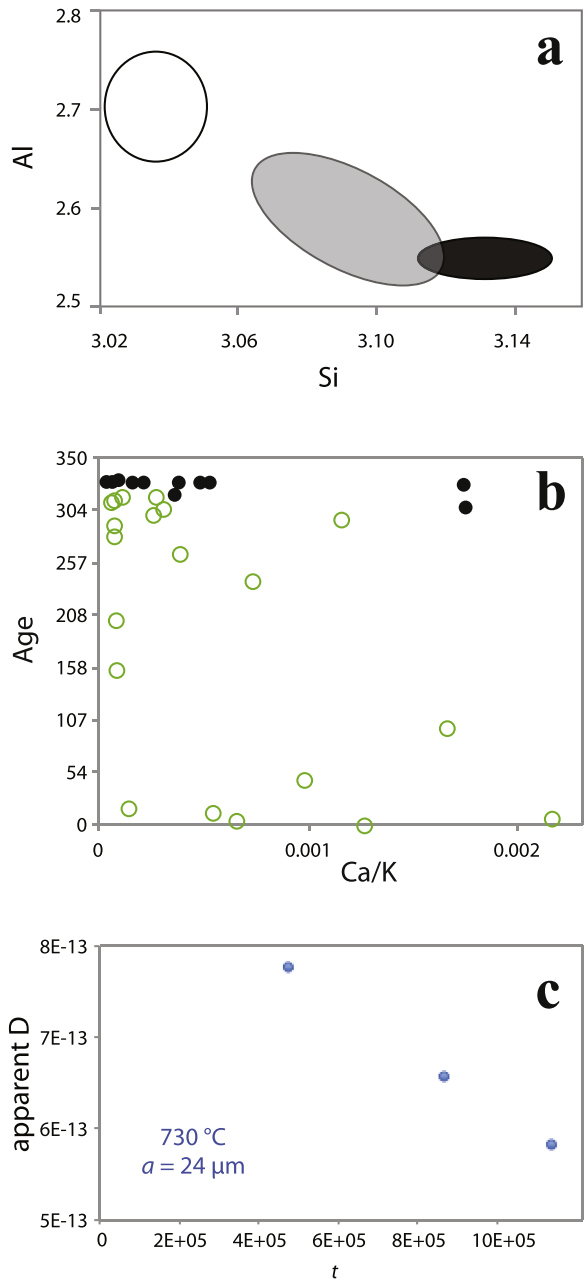

Fig. 1. Reassessment of the hydrothermal experiments by Harrison et al. (2009). (a) Chemical composition of the starting white mica (black ellipse), of the treated material (grey ellipse) and of the non-micaceous precipitates (white ellipse). Si and Al concentrations are given as atoms per formula unit (apfu). The clear trend of the grey ellipse is evidence of major open-system, heterochemical recrystallization. Redrawn after Harrison et al. (2009, their Fig. 4). (b) Common-denominator three-isotope correlation diagram of the chemical signature of the starting material (filled black circles) and of C-2342, one among the treated samples analyzed in the same laboratory (open circles). Data from Célérier (2007). The treated sample has substantially higher step Ca/K ratios, reinforcing the evidence of open-system, heterochemical recrystallization. Here, and in all other figures, element ratios are given in g/g and ages in Ma. Note that the tickmarks on the ordinate axis are not uniformly spaced, as the age is not a linear function of the (Ar/K) ratio. (c) Diagram relating the apparent diffusivity, D, of hydrothermally treated muscovite samples (data from Célérier, 2007) with the heating duration, t. The decrease of D is clear evidence that the linear trend with negative slope results from the summation of two different physical causes of Ar loss, at most one of which can be diffusion with a constant D. The heating duration is given in s and the diffusion constant in $cm^2\ s^{-1}$.

translates into a rate constant, k, which, as mentioned above, can be related to the diffusion constant D only if Fick's Law diffusion was the one and only process. In that case, $k = D/a^2$, and $D = k^*a^2$. Célérier (2007, Table 6.2) calculated D assuming a constant grain radius $a = 24$ µm. However, it could be construed that the effective diffusion radius is not the measured sieve size but the modelled parameter r, which takes into account the sizes and mass fractions of all "domains". In this assumption, the effective radius is not constant, but is smallest for low f values and gradually increases up to the sieve size only when all of the smaller domains are outgassed. It follows that in this assumption the sieve size overestimates the effective diffusion radius and therefore the product k^*a^2 is initially too high and becomes correct only at the very end of the outgassing. It thus could appear that the linear trend with negative slope reflects the mass balance of different "domains" between the leftmost point (which underwent a fractional ^{39}Ar loss $f = 0.508$: Célérier, 2007, his Table 6.2) and the rightmost one ($f = 0.651$) could reveal the gradual exhaustion of the smaller "domains". In fact, this is belied by Célérier (2007, his Table 6.3), in which he calculates that the smallest and intermediate "domains" cumulatively account for a volume fraction of 41%. By the time f has reached 50%, the smallest "domains" are completely degassed and the intermediate ones retain ca. 1.5% of their original ^{39}Ar budget. Therefore, for $f > 50\%$ the system has been practically reduced to a single-domain system, whose a no longer changes. Therefore any decrease of D/a^2 for the three samples shown in Fig. 1c reflects a decrease of D and not an increase of a. As the mathematical equations of diffusion require D to be constant, the decrease of D is clear evidence that the linear trend with negative slope results from the summation of two different physical causes of Ar loss, at most one of which can be diffusion with a constant D. This strongly suggests (albeit based only on the three mutually comparable experiments) that a time-independent Ar loss mechanism was affecting the shortest run more than the longer ones.

Finally, the Arrhenius trajectories of all twelve hydrothermal runs reported by Célérier (2007, his Fig. 6.8) are quite different from the gently kinked, nearly monotonic trajectory displayed by Harrison et al. (2009, their Fig. 9c) on a single sample, C-3051 (whose data are not presented by Célérier, 2007). None of the twelve hydrothermally treated samples reported by Célérier (2007) shows an Arrhenius trajectory even vaguely resembling the smooth trend modelled by Harrison et al. (2009) basing on C-3051. The fact that only 8% of the experimental observations fit the model calculations means that 92% do not fit it.

Even if the Cl/K discriminant is not available, some insight is provided by the Ca/K ratio, which should be zero in stoichiometric muscovite. Fig. 1b shows the CTDIC formed by the $^{37}Ar/^{39}Ar$ and $^{40}Ar^*/^{39}Ar$ ratios (i.e. Ca/K and age) of two exemplary muscovite samples from Célérier (2007). The untreated starting material, MUS-1, has the chemical signature of a muscovite with Ca-rich impurities in the typical range of average quality terrestrial samples. The Ca/K ratios of individual steps range between 0.00003 and 3.7, most steps having Ca/K < 0.00053. The first treated sample shown by Célérier (2007), C-2342, is taken as representative of all others, as it has a central role in the original discussion. Its chemical signature shows a much greater dispersion of the Ca/K ratio than the starting material. As the mass spectrometer sensitivity data are inconsistently reported, from the presented Ar isotope data it is not possible to decide whether the higher Ca/K ratio is caused by K loss, Ca gain, or both. What is clear is that open system reactions are required to account for the lack of Ca/K conservation during hydrothermal treatment. A hint comes by the visual detection of "very fine, euhedral, neoformed grains" (Célérier, 2007, p. 163). A fundamental empirical rule of prudence is that if substitution reactions are visible macroscopically, it is extremely likely that more reaction products will be found as fine-grained interstitial phases, down to the nm size (e.g. Villa et al., 1996, their Fig. 1). One could label the Ca-rich impurities as "altered domains". The expression "alteration phases" is more appropriate, as it highlights the petrogenetic unrelatedness of the pristine muscovite from its subsequent retrograde reaction

products. In any case, these alteration phases are NOT muscovite domains and must never be regressed together with true muscovite in one Arrhenius diagram (other than to show that their gas release kinetics differs from those of muscovite and causes kinked Arrhenius trajectories).

The recoil of ^{39}Ar during irradiation also produces distortions of the age spectra of very fine-grained samples (Huneke and Smith, 1976), especially clays (Fitz-Díaz et al., 2016, and references therein). In the present case, recoil certainly occurred but, as mica flakes were probably sufficiently thick, its effect did not predominate over that of recrystallization.

The reassessment of the data measured by Célérier (2007) and modelled by Harrison et al. (2009) has at least two major implications. (1) The relevance of the hydrothermal experiments to predict the Ar retentivity in natural systems is that of a strict upper limit, not that of a rate determination. Because $D < D + k$, diffusion has in any case a lower rate than the sum of diffusion + dissolution, which is what has been measured in all hydrothermal laboratory experiments on hydrous minerals to this day (see also Fig. 1c). (2) Modelling the in vacuo degassing of muscovite as caused by Fick's Law diffusion is based on the shape of age spectra; however, the TEM observations by Hess et al. (1987) show instead that the staircase-shaped age spectra reflect the formation of secondary reaction products in the hydrothermal experiment capsule. Additional evidence for the formation of secondary phases in Harrison et al.'s (2009) experiments is shown in Fig. S1. It appears that pressure enhances the formation of a non-muscovite phase more retentive of Ar than the original muscovite, which would probably have been clarified by a TEM investigation (following the classic work of Hess et al., 1987).

Harrison et al.'s (2009) model of in vacuo Fick's Law degassing of muscovite was endorsed by Kula and Spell (2012). These authors analyzed a Proterozoic muscovite separate and observed discordant age spectra, which they attributed to diffusion out of discrete muscovite "domains". However, when discussing in vacuo dehydration, they asserted that the muscovite structure remains stable despite the dehydration occurring in the octahedral layer of the TOT structure. As this is disproved by the observations of Tokiwai and Nakashima (2010) and Heller-Kallai and Lapides (2015), this incorrect assertion is not further discussed.

A closer look at the data presented by Kula and Spell (2012) reveals that they had not ensured the mathematical self-consistency of their model. First of all, most of the Ar release of the first 10–15 steps was dominated by Ca-rich impurities and not by muscovite (Fig. 2). Kula and Spell (2012) had been inferring the gas release rate of muscovite by analyzing Ca-rich contaminants, following the apparently successful strategy by Lovera et al. (1993) to ignore their own evidence that the analyzed samples were not monomineralic.

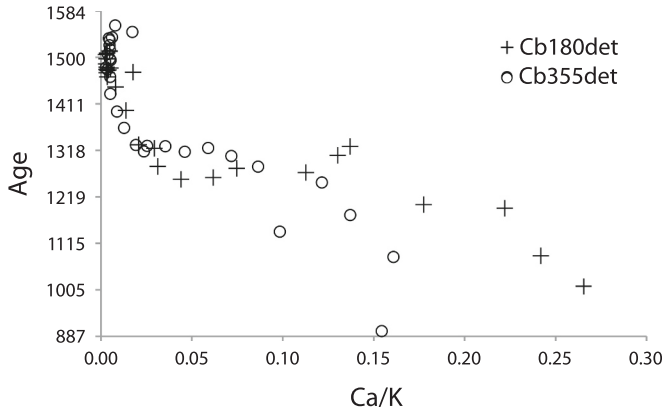

Fig. 2. Reassessment of the muscovite stepwise heating data by Kula and Spell (2012). Common-denominator three-isotope correlation diagram of the chemical signature of samples CB180 and CB355. The Ca/K ratios > 0.01 are excessively high for pure muscovite and require the degassing of Ca-rich minerals.

A further internal inconsistency are the Arrhenius trajectories (Kula and Spell, 2012, their Fig. 3), which feature a kinked shape that is asserted to be certain proof of discrete "domains" undergoing Ar loss by Fick's Law diffusion. It can be noted that the graphic representation in Fig. 3 of Kula and Spell (2012) does not match the data as presented in their Table A1; however, for the present discussion the correct absolute value of the slope is irrelevant, as it gives no useful geological prediction, and as I only will focus on the relative positions of the three sieve sizes and the breaks in slope. The three segments of the Arrhenius trajectory of the ^{39}Ar release rate reflects three different processes. In the rightmost segment (T between 500 and 700 °C) the observed heterochemical contaminants are degassed. As documented by Fig. 2, the low-temperature release comprised of the first 14 steps pertains to the degassing of high-Ca/K retrograde reaction products. The waning influence of these high-Ca/K phases is marked in Fig. 3a by the vertical dashed line at $x = 0.954$. The middle, steeper segment of the Arrhenius trajectories corresponds to the abscissa interval overlapping with the gradual structural collapse documented by Heller-Kallai and Lapides (2015), marked by the grey band. It is evident that structural collapse coincides with the highest rate of differential Ar release, and is likely causing it, as was documented for amphiboles (see above). The middle Arrhenius segments correspond to an activation energy of 350 kJ/mol, similar to (or possibly even identical, see above) to the activation energy for dehydration directly measured by Tokiwai and Nakashima (2010), 290 kJ/mol. In the leftmost region (T > 1000 °C) degassing of the corundum-K-feldspar reaction products shows lower differential rates and unsystematic Arrhenius oscillations (see also Célérier, 2007, his fig. 6.8). Note that these reaction products are expected to nucleate at the nm scale; if the sample is quenched before these phases grow above tens of μm, they will be overlooked unless a dedicated TEM investigation is performed (cfr. Hess et al., 1987; Villa et al., 1996; Chafe et al., 2014). As the reaction products do not reflect the Ar release properties of muscovite, their laboratory degassing data are not relevant to model the "cooling rate" of muscovite-bearing rocks in geological reality.

The comparison of the Arrhenius trajectories of different sieve fractions of the same sample constrains the internal consistency of the interpretive model. Fig. 3b sketches the Arrhenius trajectories predicted from Kula and Spell's (2012) model, in which samples are comprised of a number of discrete "domains" that degas following Fick's Law. Since small domains are the same independently of the sieve size, D/a^2 remains constant at low and intermediate T. Only when the smaller domains are depleted and the largest domains gradually start to dominate the Ar release the trajectories separate if the larger sieve size contains domains having a radius larger than the smaller sieve size. In the interpretation based on mineralogical observations (Fig. 3c), the effective size for diffusion is the sieve size, i.e., the micas only consist of one "domain". The degassing rates of both small and large sieve size are controlled by the same rate constant k, but because Ar release initiates at the surface the efficiency of the degassing is inversely proportional to a^2, such that the Arrhenius trajectories are parallel at low T (cfr. Chafe et al., 2014, their Fig. 6). Upon dehydration, the structural rearrangement of the octahedral mica layer erases the information on the original grain size and the Arrhenius trajectories merge. When the separately presented curves by Kula and Spell are superposed (Fig. 3a), they do not follow the prediction in Fig. 3b and instead reproduce Fig. 3c.

5. Differential Ar release plot

Early work on amphiboles (Villa et al., 1996) indicated that stepwise heating, laser ablation, and closed-system stepped etching on a widely circulated age monitor, the McClure Mountains hornblende MMhb, produced similar but not identical results, even if the age was unchanged. These observations imply that the analytical protocol chosen for the gas release did influence the shape of the age spectrum and, in

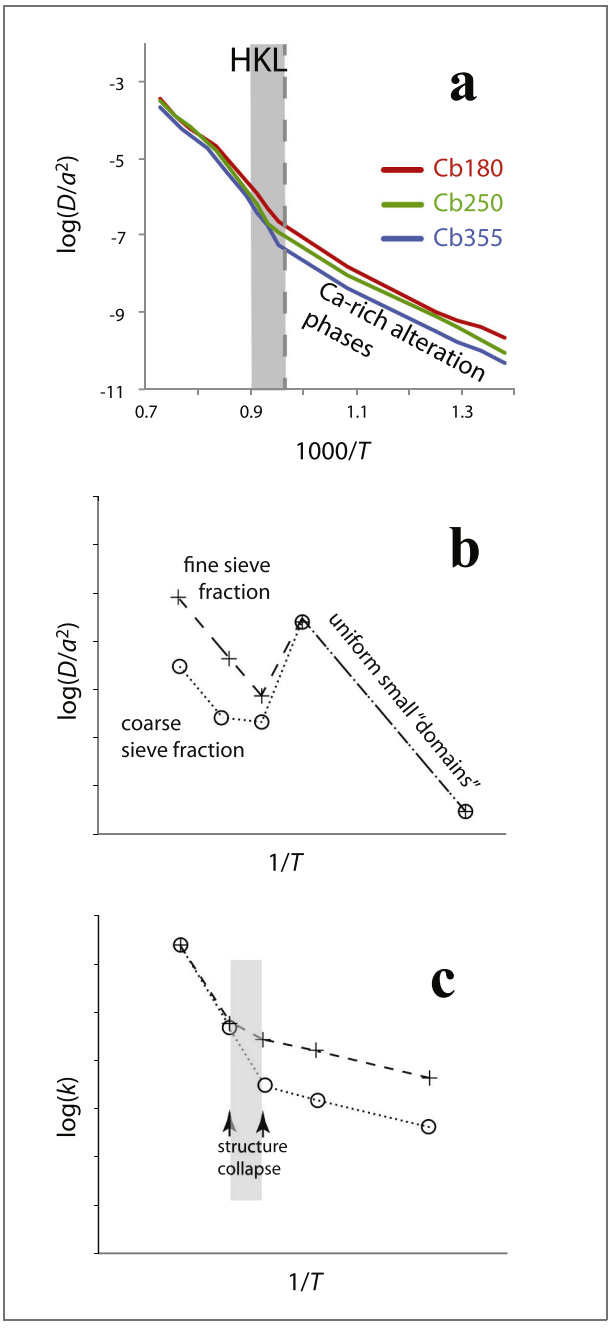

Fig. 3. Reassessment of the muscovite ^{39}Ar release data by Kula and Spell (2012). (a) Arrhenius diagram superposing the observed data of three grain-sizes of sample CB (replotted from Kula and Spell, 2012, their Fig. 3 a,c,e). The dashed grey line marks the waning importance of Ca-rich alteration phases that are present in the muscovite separate (see Fig. 2 above) and mostly degassed at $T < 850$ °C. The grey band labelled HKL marks the temperature of dehydration and ensuing structural collapse documented by Heller-Kallai and Lapides (2015). (b) Arrhenius trajectories predicted by the model used by Kula and Spell. (c) Predicted Arrhenius trajectories of two identical hydrous minerals differing only in their grainsize if their Ar release following dehydration is governed by structural collapse.

general, the degassing of Ar. Villa et al. (2000, their Fig. 3) compiled the published ^{39}Ar release data for a few "end-member" amphiboles of the Leake et al. (1997) classification. The compilation revealed that the Ar degassing rates during stepwise heating were quite variable for the different amphibole families. These observations on amphiboles (and on the polymineralic meteorites analyzed by Reynolds, 1963) are explained by first-principles physics: the collapse of a mineral structure is a function of the strength of interatomic bonds. Seeing as the amphibole family with its numerous substitutions (Leake et al., 1997) features a wide variety of bond strengths, an obvious prediction is that the peak Ar release temperature should reflect this variety, as indeed observed.

One point worth noting is that the release rates are not directly comparable as acquired, as the heating schedules are often different among samples. A normalization is therefore required, typically calculating $DR/\Delta T$, where DR is the differential release (i.e. the amount of Ar released in a step) and ΔT is the temperature increase relative to the preceding step. A delicate issue is the normalization to the duration of the heating steps, which is based on prejudicial selection of the degassing mechanism. If one assumes Fick's Law diffusion, then the correct normalization is $(DR/\Delta T)/\sqrt{t}$, where t is the step duration. However, if one assumes structural collapse, then the relevant time constant may be much shorter than the step duration. To cancel out the effect of the unknown time constant, it will be best to perform experiments designed to chart the differential release rates in various hydrated mineral families by using always the same step durations.

The data by Villa et al. (1996) on the McClure Mountains hornblende can be also displayed in a plot of the differential release of ^{37}Ar and ^{39}Ar (Fig. 4), abbreviated as DR_{37} and DR_{39}, respectively. This had already been done by Merrihue and Turner (1966) when they compared the $^{37}Ar_{Ca}$ and $^{39}Ar_{K}$ release and observed a clear bimodality in the release of the two isotopes in the Bruderheim whole rock (see above). Constant 60 min heating steps were used in the original Berkeley analytical protocol, which also called for uniform temperature increases in steps of 100 °C (Merrihue and Turner, 1966, p. 2854). This means that their Fig. 3, which plots the amount of ^{37}Ar and ^{39}Ar released in each step, also represents the normalized differential release $DR/\Delta T$ as defined here.

Two observations on the Ar release of the McClure Mountains hornblende are especially noteworthy: (1) ^{39}Ar shows two clearly resolved bursts of enhanced differential release, around 850 and 1150 °C; (2) ^{37}Ar is released in only one burst around 1150 °C. The interpretation of these observations is straightforward in light of the mineralogical constraints. Electron microscopy of the analyzed sample documented the presence of biotite (Villa et al., 1996), often intergrown at the (sub-)μm scale. Because of the stoichiometry of biotite (high K and low Ca), a few modal percent biotite can have a large effect on the total ^{39}Ar concentration of the hornblende separate, all while not affecting the total ^{37}Ar concentration. The peak of the ^{39}Ar release in the heating steps between 800 and 900 °C is accompanied by the lowest Ca/K ratio, providing the identification of these steps as due to biotite intergrowths. The release of ^{37}Ar and ^{39}Ar together in the steps between 1000 and 1300 °C is evidence that an entirely different phase is releasing its Ar, with an approximately constant Ca/K ratio. It is well documented that hornblende undergoes several sequential reactions precisely in that

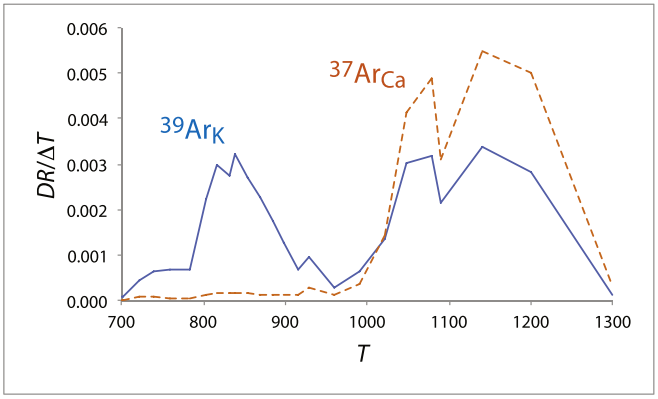

Fig. 4. Differential release of ^{37}Ar and ^{39}Ar, normalized to the temperature increase between two successive steps, of the McClure Mountains hornblende analyzed by Villa et al. (1996). The unit of the ordinate axis is %/°C.

temperature interval (Wartho et al., 1991; Lee et al., 1991; Lee, 1993; Wartho, 1995). The combination of the mineralogical evidence with the Ar release data forces the conclusion that Ar is released from the hornblende *because* its crystal structure, and the interatomic distance that limits the transport of Ar, is abruptly modified by these reactions. An Arrhenius diagram (Villa et al., 1996, p. 78) features breaks in slope coinciding with the known structural rearrangements. Note that the ordinate of the Arrhenius diagram is calculated from the Ar release data, and as such it should be termed "degassing rate *k*". Calling the degassing rate "diffusivity *D*" is a misnomer, as Fick's Law requires an inert matrix; macroscopic mathematical descriptions of diffusion (Crank, 1975) can account for variable boundary conditions but not for time-dependent matrix variations. The temperature dependence of *k* reflects the temperature-dependent progress of the in vacuo reactions that rearrange the crystal structure and thus control the Ar release.

A further implication of the comparison between different degassing protocols is the scale at which they can extract geochronological information from the analyzed mineral. Villa et al. (1996, their Fig. 5) illustrated the size of the microstructural features accessible by the UV laser analysis. Each pit ablated a volume of ca. 50000 μm^3. Even if depth profiling can achieve a vertical resolution of a few μm, the high depth resolution comes at the price of a large surface pit. The limiting factor is not the possibility to focus a laser beam to produce a (sub-)μm pit, capable of interrogating μm-scale zoning or inclusions, but the necessity to obtain a sufficient number of Ar atoms for a reasonably precise measurement. The tradeoff between precision and accuracy lies precisely in the size of the microstructures that carry petrochronological information: if the size of the microstructures is <50000 μm^3, the laser analysis will be inaccurate to the extent that it mixes the Ar from different, unrelated sources. The UV laser data on the heated McClure Mountain hornblende do show some rejuvenation but cannor pinpoint it to the biotite inclusions, as these can be as small as 1 μm^3. On the other hand, stepwise heating of the same amphibole is able to exploit the diathermal collapse of the biotite and amphibole structure, regardless of the size of the inclusion. Potentially this could achieve a spatial resolution of 1 nm^3; however, the realities of recoil (Huneke and Smith, 1976; Onstott et al., 1995) limit the achievable spatial resolution to ca. $(0.1\ \mu m)^3$, below which size the recoiling Ar atoms are redistributed and the identities of the analyzed phases are jumbled. A similar issue with comparing the real spatial resolution of in situ dating by UV laser with

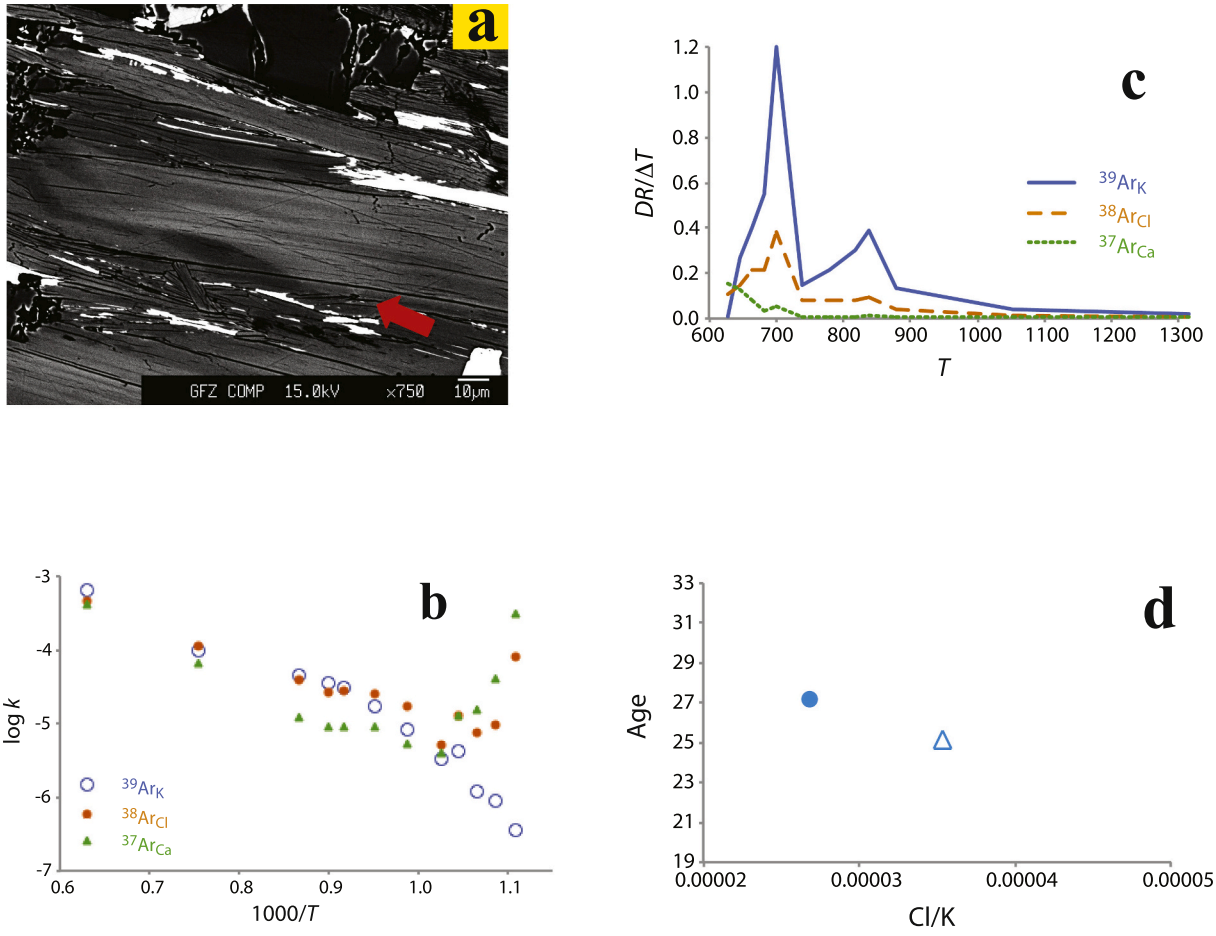

Fig. 5. Four complementary pieces of information on white mica N-001 from Naxos, whose context is required for a reliable geological interpretation. (a) Backscattered electron image. Muscovite replacing phengite is visible at a scale much smaller than the scale bar (10 μm). In addition to phengite and muscovite, the sample contains very fine late alteration "clays" (arrow). (b) Arrhenius diagram showing the rate constant *k* of the release of ^{39}Ar (open blue circles), ^{38}Ar (filled orange circles) and ^{37}Ar (green triangles). The rates of the low-temperature ^{37}Ar and ^{38}Ar release are up to three orders of magnitude higher than that of ^{39}Ar and define positive Arrhenius slopes. This effect cannot be satisfactorily explained by ultrasmall "diffusion domains". In fact, it is the manifestation of the heterochemical Ca + Cl-rich alteration phases documented in Fig. 5a. (c) Superposed differential release plot for ^{39}Ar (solid blue line), ^{38}Ar (dashed orange line) and ^{37}Ar (dotted green line). The degassing peak of the retrogressive muscovite is very prominent; the relict phengite generation degasses at a higher temperature. (d) Common-denominator age-Ca/K plot. The open triangle represents the 701 °C step corresponding to the first ^{39}Ar release peak, the filled circle represents the 838 °C step, the second ^{39}Ar release peak. Both age and chemical composition are slightly but resolvably different, in agreement with the independent petrologic constraints (Fig. 5a) and complementing the differential Ar release plot in Fig. 5c. (For interpretation of the references to colour in this figure legend, the reader is referred to the web version of this article.)

the effective spatial resolution provided by stepwise heating was documented by Müller et al. (2002).

In micas, especially in white mica, the compositional variety is much lower than that of amphiboles, and the effect of bond strength variability on the differential Ar release is expected to be smaller. Nevertheless, some variation in the integrated Ar release rate had been documented by Wijbrans and McDougall (1986, their Fig. 5). As the original samples were not available for duplicate measurements, a new, as yet unpublished white mica sample from Naxos, N-001, was sampled <500 m from the two original Wijbrans and McDougall (1986) samples 81–584 and 81–535, which both clearly exhibit the mixing between an early phengite and a later partial retrogression to muscovite. Sample N-001 was first studied by EPMA, which confirmed the observations of a phengite-muscovite mixture; the size of the retrograde muscovite is only visible by EPMA, as the replacement layers can be <1 μm thick (Fig. 5a). In addition to the two mica generations, traces of alteration minerals, dubbed "clays" in the petrological literature (Putnis, 2009; Hellmann et al., 2012), are observed at the rims of the mica grains.

Stepwise heating of N-001 followed the protocol in Villa et al. (2000). Data are presented in Table S1. An Arrhenius diagram can be displayed to chart the temperature dependence of the degassing rate of $^{39}Ar_K$, $^{37}Ar_{Ca}$ and $^{38}Ar_{Cl}$. Fig. 5b shows the Arrhenius trajectories of all three displayed Ar isotopes. Taken out of context, the kinked Arrhenius trajectory of the ^{39}Ar release could be modelled as caused by the degassing of small "domains" (Harrison et al., 2009; Kula and Spell, 2012). However, in a homogeneous matrix consisting only of one mineral species of uniform composition, the degassing of all isotopes must be the same. On the contrary, the observation is that the two often "neglected" isotopes $^{37}Ar_{Ca}$ and $^{38}Ar_{Cl}$, which proxy for the chemical composition, follow very different Arrhenius trajectories. Both isotopes feature an ordinate value for the first release steps higher by ca. 3 orders of magnitude than that of ^{39}Ar, followed by a positive Arrhenius slope as T increases. Only at $T > 700$ °C do the three Arrhenius trajectories become closer to each other. If the high Ar release rates of $^{37}Ar_{Ca}$ and $^{38}Ar_{Cl}$ at $T < 700$ °C are modelled in terms of a "domain" size distribution, this immediately becomes inconsistent with the observation that the small "domains" are not isochemical with the larger ones, degassed at $T > 700$ °C. The information on the degassing rate below 700 °C must not be regressed together with the high-temperature steps, as they pertain to entirely different minerals.

The visualization of the Ar release chosen by Wijbrans and McDougall (1986) on samples nearly equivalent to N-001 can be made pithier by plotting the normalized differential release $DR/\Delta T$, as shown in Fig. 5c. The differential ^{39}Ar release shows two clearly separated peaks of the degassing rate at furnace temperatures of 701 and 838 °C. The differential release can be plotted for any Ar isotope, including the neglected isotopes $^{37}Ar_{Ca}$ and $^{38}Ar_{Cl}$. In the case of white mica N-001, the release patterns of $^{37}Ar_{Ca}$ and $^{38}Ar_{Cl}$ are shown together with that of $^{39}Ar_K$ in Fig. 5c. For $T \leq 665$ °C, the three release patterns appear completely discordant among each other, confirming a substantial chemical, and therefore mineralogical, heterogeneity. Between 680 and 880 °C, two prominent degassing peaks are observed, in which all three isotopes show similar (but not identical: see below) degassing patterns and peak height ratios. The peak centred at 701 °C is identified as the retrogressive muscovite; the relict phengite generation, which degasses at a higher temperature (Wijbrans and McDougall, 1986, their Fig. 5), has a peak centred at 838 °C. At $T \geq 900$ °C, the complete dehydration temperature (cfr. Heller-Kallai and Lapides, 2015), the differential release of all three Ar isotopes drops to near zero, as the white mica proper has been efficiently outgassed by the major structural rearrangement. This implies that the portion of the Arrhenius diagram of Fig. 5b with $x < 0.85$ in does not pertain to either muscovite or phengite and ought to be disregarded when studying the diffusivity of white micas.

The straightforward observation that the release of the three Ar isotopes is markedly different provides very strict constraints on any interpretation. The prerequisite petrological characterization (Fig. 3a) has not revealed a monomineralic mica, but on the contrary a phengite-muscovite-clay(s) polymineralic mix. Therefore, the Arrhenian ordinate k is not the single-phase diffusivity but a composite degassing rate, summing the degassing rates of all individual components of the mix.

What is proposed here instead of "domain" modelling is a way to interpret the observations in a mutually supporting context. Firstly, the polymineralic nature of white mica N-001 is ascertained by EPMA. This observation cascades on two complementary visualizations of the Ar isotope data: (i) the degassing sequence of the constituents of the mixture is revealed by the differential release of $^{39}Ar_K$, $^{37}Ar_{Ca}$ and $^{38}Ar_{Cl}$; (ii) the EPMA observation that the mixture is comprised of heterochemical phases is confirmed by the chemical Ca/K and Cl/K signature displayed in a CDTIC. As an example, the Cl/K signature and age of the two DR_{39} peaks of the N-001 phengite-muscovite mixture are shown in Fig. 5d. The 701 °C peak (muscovite) has a Cl/K ratio higher by 50% than the phengite peak (838 °C), as visible also from the different relative heights of DR_{38} and DR_{39}. The Cl/K ratio and the age are negatively correlated: the high-Cl 701 °C step is younger by 2 Ma than the low-Cl 838 °C step. All of these three interpretive pathways are combined in an internally consistent petrochronological reconstruction capable of deconvolving the age of the high pressure phengite from the age of the subsequent retrogression to muscovite.

6. Conclusions

As the physics of dehydration and consequent structural collapse depends on a large number of parameters, it could appear that many interpretive models are potentially adequate descriptions of the Ar degassing pattern of hydrous minerals. However, a key feature of any model must be internal consistence and external consistence with independent petrological constraints. The models based on Fick's Law diffusion out of hydrous, monomineralic samples, with the assumption of discrete "diffusion domains" in order to account for non-linear Arrhenius trajectories, are neither internally nor externally consistent. Instead, it is necessary to both account for structural breakdown of hydrated minerals during in vacuo heating and to account for the presence of heterochemical retrograde reaction products. This can be achieved by combining common-denominator three-isotope correlation diagrams and differential Ar release plots, which together provide an internally and externally consistent interpretive approach.

Supplementary data to this article can be found online at https://doi.org/10.1016/j.chemgeo.2021.120076.

Declaration of Competing Interest

The authors declare that they have no known competing financial interests or personal relationships that could have appeared to influence the work reported in this paper.

Acknowledgements

Thanks are due to Johannes Glodny for the BSE image, and to Thomas Nägler for a preliminary critical reading of the manuscript. Constructive reviews by Chris Hall and two anonymous referees are gratefully acknowledged. Happy 75th birthday, Jan Dirk.

References

Airaghi, L., Warren, C.J., de Sigoyer, J., Lanari, P., Magnin, V., 2018. Influence of dissolution/reprecipitation reactions on metamorphic greenschist to amphibolite facies mica $^{40}Ar/^{39}Ar$ ages in the Longmen Shan (eastern Tibet). J. Metamorph. Geol. 36, 933–958.

Akker, I.V., Berger, A., Zwingmann, H., Todd, A., Schrank, C.E., Jones, M.W.M., Kewish, C.M., Schmid, T.C., Herwegh, M., 2021. Structural and chemical resetting mechanisms in white mica and their effect on K-Ar data during low temperature metamorphism. Tectonophysics 800, 228708.

Allaz, J., Berger, A., Engi, M., Villa, I.M., 2011. The effects of retrograde reactions and of diffusion on ^{39}Ar-^{40}Ar ages of micas. J. Petrol. 52, 691–716.
Allsopp, H.L., 1961. Rb-Sr age measurements on total rock and separated mineral fractions from old granite of the central transvaal. J. Geophys. Res. 66, 1499–1508.
Baadsgaard, H., Campbell, F.A., Folinsbee, R.E., Cumming, G.L., 1961. The Bruderheim meteorite. J. Geophys. Res. 66, 3574–3577.
Bergstrom, C.T., West, J.D., 2020. Calling Bullshit. Random House, New York (319 pp. ISBN 9780593229767).
Bosse, V., Villa, I.M., 2019. Petrochronology and hygrochronology of tectono-metamorphic events. Gondwana Res. 71, 76–90.
Célérier, J., 2007. The Structural and Thermal Evolution of the Kumaon and Garwhal (*sic*) Lesser Himalaya, India. PhD Thesis. Australian National University. https://openresearch-repository.anu.edu.au/handle/1885/149627 (accessed on 2020.12.20).
Chafe, A.N., Villa, I.M., Hanchar, J.M., Wirth, R., 2014. A re-examination of petrogenesis and ^{40}Ar/^{39}Ar systematics in the the Chain of Ponds K-feldspar: "diffusion domain" archetype versus polyphase hygrochronology. Contrib. Mineral. Petrol. 167 (5), 1–17 paper 1010.
Crank, J., 1975. Mathematics of Diffusion, Second edition. Clarendon Press, Oxford. (488 pp.).
Dahl, P.S., 1997. A crystal-chemical basis for Pb retention and fission-track annealing systematics in U-bearing minerals, with implications for geochronology. Earth Planet. Sci. Lett. 150, 277–290.
Duke, M., Maynes, D., Brown, H., 1961. The petrography and chemical composition of the Bruderheim meteorite. J. Geophys. Res. 66, 3557–3563.
Fitz-Díaz, E., Hall, C.M., van der Pluijm, B.A., 2016. XRD-based ^{40}Ar/^{39}Ar age correction for fine- grained illite, with application to folded carbonates in the Monterrey Salient (northern Mexico). Geochim. Cosmochim. Acta 181, 201–216.
Foland, K.A., 1983. ^{40}Ar/^{39}Ar incremental heating plateaus for biotites with excess argon. Chem. Geol. 41, 3–21.
Gaber, L.J., Foland, K.A., Corbató, C.E., 1988. On the significance of argon release from biotite and amphibole during ^{40}Ar/^{39}Ar vacuum heating. Geochim. Cosmochim. Acta 52, 2457–2465.
Hall, C.M., 2014. Direct measurement of recoil effects on ^{40}Ar/^{39}Ar standards. Geol. Soc. Lond. Spec. Publ. 378, 53–62.
Harrison, T., Célérier, J., Aikman, A.B., Hermann, J., Heizler, M.T., 2009. Diffusion of ^{40}Ar in muscovite. Geochim. Cosmochim. Acta 73, 1039–1051.
Heller-Kallai, L., Lapides, I., 2015. Dehydroxylation of muscovite: study of quenched samples. Phys. Chem. Miner. 42, 835–845.
Hellmann, R., Wirth, R., Daval, D., Barnes, J.-P., Penisson, J.-M., Tisserand, D., Epicier, T., Florin, B., Hervig, R.L., 2012. Unifying natural and laboratory chemical weathering with interfacial dissolution– reprecipitation: a study based on the nanometer-scale chemistry of fluid–silicate interfaces. Chem. Geol. 294-295, 203–216.
Hess, J.C., Lippolt, H.J., Wirth, R., 1987. Interpretation of ^{40}Ar/^{39}Ar spectra of biotites - evidence from hydrothermal degassing experiments and TEM studies. Chem. Geol. 66, 137–149.
Hodges, K.V., Hames, W.E., Bowring, S.A., 1994. ^{40}Ar/^{39}Ar age gradients in micas from a high-temperature-low-pressure metamorphic terrain; evidence for very slow cooling and implications for the interpretation of age spectra. Geology 22, 55–58.
Huneke, J.C., Smith, S.P., 1976. The realities of recoil: ^{39}Ar recoil out of small grains and anomalous age patterns in ^{39}Ar-^{40}Ar dating. In: Proceedings of the Lunar Science Conference 7th, 1987-2008.
Kula, J., Spell, T.L., 2012. Recovery of muscovite age gradients by ^{40}Ar/^{39}Ar vacuum furnace step-heating analysis. Chem. Geol. 304-305, 166–174.
Laves, F., 1956. Über die Bedeutung der Barbierit-Analbit-Umwandlung (displacive transformation) für die Erscheinungsformen der Feldspäte in Larvikiten und Rhombenporphyren. Z. Krist. 107, 196–201.
Leake, B.E., Woolley, A.R., Arps, C.E.S., Birch, W.D., Gilbert, M.C., Grice, J.D., Hawthorne, F.C., Kato, A., Kisch, H.J., Krivovichev, V.G., Linthout, K., Laird, J., Mandarino, J.A., Maresch, W.V., Nickel, E.H., Rock, N.M.S., Schumacher, J.C., Smith, D.C., Stephenson, N.C.N., Ungaretti, L., Whittaker, E.J.W., Guo, Y.Z., 1997. Nomenclature of amphiboles: report of the subcommittee on amphiboles of the International Mineralogical Association, commission on new minerals and mineral names. Eur. J. Mineral. 9, 623–651.
Lee, J.K.W., 1993. The argon release mechanisms of hornblende in vacuo. Chem. Geol. 106, 133–170.
Lee, J.K.W., Onstott, T.C., Cashman, K.V., Cumbest, R.J., Johnson, D., 1991. Incremental heating of hornblende in vacuo: implications for ^{40}Ar/^{39}Ar geochronology and the interpretation of thermal histories. Geology 19, 872–876.
Lovera, O.M., Heizler, M.T., Harrison, T.M., 1993. Argon diffusion domains in K-feldspar II: kinetic properties of MH-10. Contrib. Mineral. Petrol. 113, 381–393.
Merrihue, C.M., Turner, G., 1966. Potassium-argon dating by activation with fast neutrons. J. Geophys. Res. 71, 2852–2857.
Müller, W., Kelley, S.P., Villa, I.M., 2002. Dating fault-generated pseudotachylytes: Comparison of ^{40}Ar/^{39}Ar stepwise-heating, laser-ablation and Rb/Sr microsampling analyses. Contributions to Mineralogy and Petrology 144, 57–77.
Naumenko-Dèzes, M., Nägler, T.F., Villa, I.M., Mezger, K., 2018. ^{40}K-^{40}Ca – ^{87}Rb-^{87}Sr age comparison: constraints on the ^{40}K decay constant. Geochim. Cosmochim. Acta 220, 235–247.
Nicolaysen, L.O., 1961. Graphic interpretation of discordant age measurements on metamorphic rocks. Ann. N. Y. Acad. Sci. 91 (2), 198–206.
Onstott, T.C., Miller, M.L., Ewing, R.C., Arnold, G.W., Walsh, D.S., 1995. Recoil refinements: implications for the ^{40}Ar/^{39}Ar dating technique. Geochim. Cosmochim. Acta 59, 1821–1834.
Parsons, I., Brown, W.L., Smith, J.V., 1999. ^{40}Ar/^{39}Ar thermochronology using alkali feldspars: real thermal history or mathematical mirage of microtexture? Contrib. Mineral. Petrol. 136, 92–110.
Phillips, D., Onstott, T.C., 1988. Argon isotopic zoning in mantle phlogopite. Geology 16, 542–546.
Pruett, R.J., Pickering Jr., S.M., 2006. Kaolin. In: Kogel, J.E., Trivedi, N.C., Barker, J.M., Krukowski, S.T. (Eds.), Industrial Minerals & Rocks, 7th ed., pp. 383–399.
Putnis, A., 2009. Mineral replacement reactions. Rev. Mineral. Geochem. 70, 87–124.
Raase, P., 1974. Al and Ti contents of hornblende, indicators of pessure and temperature of regional metamorphism. Contrib. Mineral. Petrol. 45, 231–236.
Reynolds, J.H., 1963. Xenology. J. Geophys. Res. 68, 2939–2956.
Sletten, V.W., Onstott, T.C., 1998. The effect of the instability of muscovite during in vacuo heating on ^{40}Ar/^{39}Ar step-heating spectra. Geochim. Cosmochim. Acta 62, 123–141.
Tokiwai, K., Nakashima, S., 2010. Dehydration kinetics of muscovite by in situ infrared microspectroscopy. Phys. Chem. Miner. 37, 91–101.
Turner, G., 1968. The distribution of potassium and argon in chondrites. In: Ahrens, L.H. (Ed.), Origin and Distribution of the Elements. Pergamon Press, New York, pp. 387–398.
Turner, G., Miller, J.A., Grasty, R.L., 1966. The thermal history of the Bruderheim meteorite. Earth Planet. Sci. Lett. 1, 155–157.
Turner, G., Huneke, J.C., Podosek, F.A., Wasserburg, G.J., 1971. ^{40}Ar-^{39}Ar ages and cosmic ray exposure age of Apollo 14 samples. Earth Planet. Sci. Lett. 12, 19–35.
Villa, I.M., 2016. Diffusion in mineral geochronometers: present and absent. Chem. Geol. 420, 1–10.
Villa, I.M., Hanchar, J.M., 2017. Age discordance and mineralogy. Am. Mineral. 102, 2422–2439.
Villa, I.M., Puxeddu, M., 1994. Geochronology of the Larderello geothermal field: new data and the "closure temperature" issue. Contrib. Mineral. Petrol. 115, 415–426.
Villa, I.M., Grobéty, B., Kelley, S.P., Trigila, R., Wieler, R., 1996. Assessing Ar transport paths and mechanisms for McClure Mountains Hornblende. Contrib. Mineral. Petrol. 126, 67–80.
Villa, I.M., Hermann, J., Müntener, O., Trommsdorff, V., 2000. ^{39}Ar-^{40}Ar dating of multiply zoned amphibole generations (Malenco, Italian Alps). Contrib. Mineral. Petrol. 140, 363–381.
Villa, I.M., Bucher, S., Bousquet, R., Kleinhanns, I.C., Schmid, S.M., 2014. Dating polygenetic metamorphic assemblages along a transect through the Western Alps. J. Petrol. 55, 803–830.
Villa, I.M., 2010. Disequilibrium Textures vs Equilibrium Modelling: Geochronology at the Crossroads. In: Spalla, M.I., Marotta, A.M., Gosso, G. (Eds.), Advances in Interpretation of Geological Processes. Geol. Soc., London, pp. 1–15. Spec. Pub. 332.
Wartho, J.A., 1995. Apparent argon diffusive loss ^{40}Ar/^{39}Ar age spectra in amphiboles. Earth Planet. Sci. Lett. 134, 393–407.
Wartho, J.A., Dodson, M.H., Rex, D.C., Guise, P.G., 1991. Mechanisms of Ar release from Himalayan metamorphic hornblende. Am. Mineral. 76, 1446–1448.
Wijbrans, J.R., McDougall, I., 1986. ^{40}Ar/^{39}Ar dating of white micas from an Alpine high-pressure metamorphic belt on Naxos (Greece): the resetting of the argon isotopic system. Contrib. Mineral. Petrol. 93, 187–194.
Zimmermann, J.-L., 1970. Contribution à l'étude de la déshydratation et de la libération de l'argon des micas. Geochim. Cosmochim. Acta 34, 1327–1350.